Rev. Adv. Mater. Sci. 39 (2014) 25-33

KINETICS OF NECK FORMATION DURING NANOPARTICLE SINTERING: APPROACH OF DIMENSIONALITY REDUCTION

Amlan Dutta

S. N. Bose National Centre for Basic Sciences, Block – JD, Salt Lake, Kolkata-700098, India

Received: June 23, 2014

Abstract. The present study proposes the use of principal component analysis as a robust method of reducing the effective dimensionality of a multivariate time-series dataset, to analyze the underlying kinetics of a process studied by molecular dynamics simulations. As a proof of concept, this technique has been applied to explore the mechanism of neck formation during the sintering of two gold nanoparticles. It is found that the method of dimensionality reduction provides an intuitive and simple one-dimensional representation of this complex process, using which the quantities like rate of the process, thermodynamic forces and effective inertia can be evaluated. Both isothermal sintering and linear heating have been simulated and the fundamental differences between the kinetics of these two cases have been highlighted.

1. INTRODUCTION

Over the last several years, a steep rise in the research activities on various nanosized particles has led to wide interest in the process of their sintering, not only from the standpoint of applications but of the basic physics of materials as well. One class of studies [1-3] is motivated by the positive role played by the process of nanosintering, particularly in the fabrication of high conductance contacts on flexible substrates, whereas another class [4,5] views it as an antagonistic agent on account of its negative impact on the efficacy of nanocatalysts. In any case, it is generally agreed upon that due to significant atomic forces and curvature-driven diffusion, sintering of ultrasmall particles follow the kinetics which is substantially distinct from those proposed for the coarser particles [6-8]. Despite the attempts like synchrotron x-ray studies [9], it remains extremely difficult to experimentally probe the kinetics of nanosintering, especially during the initial stage of neck formation, which can take place in a few picoseconds even at temperature much below the melting point [7,10]. Under such limitations, the atomistic simulations have offered enormous advantage on account of their ability to furnish length and time resolutions over a broad range. Accordingly, numerous investigations have been reported, which belong to several categories of simulations like two-particle sintering [7,8,11], three-particle sintering [12], particle-chain sintering [13], diffusive molecular dynamics [14], etc.

One major issue with the molecular dynamics (MD) simulations of nanosintering is that even though the terms like “state of the system” and “thermodynamic forces” are often encountered in the context of kinetics, it is difficult to quantify these intuitive notions with atomistic precision. Therefore, instead of utilizing the entire atomistic data to specify the state of the system, somewhat cruder expressions like neck-radius, curvature and radius of gyration are taken into account [7,8,15]. The primary hindrance here can be recognized as the large dimensionality required for describing the systems under study. The configuration or structural state of a system containing n atoms requires $3n$ variables for its expression, where n can be of the order of hundreds

Corresponding author: Amlan Dutta, e-mail: amlan.dutta@bose.res.in

or thousands even for an ultrasmall nanoparticle. Clearly, understanding the evolution of the state directly through this accurate but large pool of numerical raw data goes beyond the limits of general human comprehension. The present study is aimed at proposing an alternative method of processing the atomistic data such that the numerical output of the MD simulations can become more heuristic and interpretable quantitatively. By means of the rigorous method of principal component analysis (PCA) as an efficient tool of dimensionality reduction, the multivariate atomistic data of nanosintering has been shown to be compressible to the monovariate states, which in effect, can be employed to quantify the so called "thermodynamic forces" on the system. As a proof of concept, this technique has been applied to the process of necking observed by means of molecular dynamics simulations of sintering of gold nanoparticles (AuNPs). Although the results shown here belong to a specific case study, the method of dimensionality reduction is inherently a general one and can be equally valid across a broad range of simulation based studies.

2. SCHEME OF SIMULATION

The MD simulations performed here are the typical two-particle simulations with the spherical metallic particles of 5 nm diameters. The particles are modelled by using an EAM type potential of gold developed by Adams *et al.* [16]. Both the particles are initially separated by a large gap and thermally equilibrated at the desired temperature. Once properly thermalized, the particles are brought closer to each other within a small distance of 2 Å and the process of nanosintering initiates. In the present study, two sets of simulations are performed. The first one involves isothermal sintering at three different temperatures of 550K, 600K, and 650K. The second simulation consists of heating the closely spaced nanoparticles from 50K to 650K at a constant rate of 3 K/ps, mimicking the rapid laser sintering. The formation of neck starts almost immediately and proceeds at a rapid rate for a few tens of picoseconds. In both of these cases, the simulations proceed till the initial neck formation is complete. Nevertheless, as pointed out earlier, the tool of PCA is intrinsically very flexible and can easily be employed for the later stages of sintering as well. As the neck growth occurs more rapidly in the first few picoseconds and slows down at a later stage, the atomic coordinates can initially be dumped with larger frequency for the first several thousand time steps, whereas the dumping rate can be reduced during the later part of the simulation. During the course of the simulations, temperature is controlled by means of the Nosé-Hoover thermostat [17,18] and the atomic trajectories are computed with a time resolution of 1 fs. The open source MD code LAMMPS (http://lammps.sandia.gov) [19] has been used for generating the atomic trajectories, which are further analyzed as described in the next sections.

3. PRINCIPAL COMPONENT ANALYSIS

The statistical tool of principal component analysis (PCA) [20] employed in the present study is based upon the robust principles of linear dimensionality reduction and is considered as the discrete form of Karhunen-Loève transform. The primary goal of PCA is to obtain the evolution of a multidimensional physical quantity expressible with a large number of dimensions or components, and transform it into another derived trajectory of the same quantity that can now be specified with only a few effective components. Here the 'effectiveness' of a component is understood in terms of the variance of the physical quantity along that component. In other words, the basic idea here is to obtain a large dataset as multivariate time-series and transform it to a new set of orthogonal basis vectors such that the variances of the dataset in this new coordinate system are optimized. In an atomistic simulation like molecular statics or dynamics, the position of a single atom is specified through three components. Accordingly, the instantaneous structure of a system consisting of n atoms can be fully described by a vector $\mathbf{r}$ of $3n$ dimensions and therefore, the structural evolution of the atomistic system can be considered as the trajectory of $\mathbf{r}$ in a $3n$-dimensional vector space. Once this trajectory is obtained, the following steps are followed to perform the PCA of the atomistic data.

Step 1: Matrix representation of trajectory – If the coordinates of the atoms are sampled at N_s discrete intervals, the entire time evolution of the structure can be represented by the $N_s \times 3n$ matrix,

$$D = \begin{bmatrix} \boldsymbol{r}_1 \\ \boldsymbol{r}_2 \\ \vdots \\ \boldsymbol{r}_{N_s} \end{bmatrix}.$$

Step 2: Mean-centering – A new matrix Δ is derived from D by subtracting the mean value of each of the

3*n* columns, from the corresponding elements of that column. Thus the operation,

$$\Delta_{ij} = D_{ij} - \frac{\sum_{i=1}^{N_s} D_{ij}}{N_s},$$

causes the columns of Δ to be mean-centered. Although the operation of mean-centering is sufficient to carry out the next steps of PCA, it is often prescribed to use a well conditioned dataset, which involves rescaling of the dataset to normalize the variances of each column of Δ, in addition to the usual mean-centring.

Step 3: Computing the covariance-matrix – The $3n \times 3n$ covariance matrix is obtained as $C = \Delta^T\Delta$, where Δ^T denotes the transpose of Δ. As Δ has been obtained by mean-centering the original dataset *D*, off-diagonal elements of *C* represent the various covariances of the components of **r**, while the 3*n* variances occupy diagonal positions.

Step 4: Diagonalizing the covariance-matrix – We can now define an eigenvector **d,** satisfying the eigenvalue equation, $C\mathbf{d} = \lambda\mathbf{d}$, where λ is an eigenvalue. This equation has *3n* solutions and can be solved by diagonalizing the matrix *C*, thereby yielding a diagonal matrix with the eigenvalues as $C^{diag} = diag(\lambda_1, \lambda_2, ..., \lambda_{3n})$, such that $\lambda_1 > \lambda_2 > ... > \lambda_{3n}$.

The unit vector along $\mathbf{d}_1$, corresponding to the largest eigenvalue λ_1, is known as the principal direction (or axis). If λ_1 is much larger than the rest of the eigenvalues, it indicates that instead of taking into account the entire multivariate dataset, it is sufficient to consider only the projection of the trajectory, $\mathbf{s}(t)$, on the principal axis [20]. Thus, it is possible to compress the 3*n*-dimensional vector time-series to a single-variable trajectory, $S(t) = \mathbf{s}(t).\mathbf{d}_1$, which better serves the purpose of intuitive comprehension and thermodynamic analysis. In addition, this technique is also capable of filtering out the noise present in the system, provided that the time duration over which the atomic trajectory has been acquired, is much larger than the time scale of the noise fluctuations. This is made feasible, for the eigenvalues affected by the noise become insignificantly small and are placed away from the principal eigenvalue in the eigenvalue spectrum. Hence their effect on the principal projection $S(t)$ is negligibly small and the data becomes almost completely free of the noise. The method of PCA has already been proved to be much prolific across a broad range of applications ranging from finance to image processing [21-23]. In the recent years, it has also witnessed exciting successes in some fields of material science like ferroelectric relaxors [24] and the quasistatic behaviour of dislocation cores [25].

4. RESULTS AND DISCUSSION

In the present simulations of nanosintering, formation of neck is primarily driven by the surface diffusion of atoms of the AuNPs. Therefore, only the atomic trajectories in the 0.5 nm thick outer shells of the nanoparticless have been used for the purpose of PCA. In the sintering simulations of 5 nm particles, the outer shells have 3812 atoms in total, which correspond to the specifications of states as 11436-dimensional vectors. The time-series of these states are generated from the atomic coordinates of the systems, and the eigenvalues, eigenvectors and transformed datasets are computed by the procedure explained in the previous section. For isothermal sintering simulations, the largest eigenvalues (λ_1), after normalizing with respect to sum of all the eigenvalues, are found to be in excess of 90%, whereas the MD computation simulating the steady elevation in temperature yields about 77% as the normalized principal eigenvalue. Such large values imply that out of thousands of variables, the principal eigenvalues effectively account for the major portion of the variances of the MD data and hence, the principal projections, ($S(t)$), of the multivariate datasets ($\mathbf{s}(t)$) can alone represent the states of the system with reasonable precision.

Figs. 1a and 1b show the evolution of the principal coordinates with time under the conditions of isothermal and linear heating respectively. We can observe that for both the cases, $S(t)$ increases rapidly with time for the first 20 – 30 ps irrespective of the temperature, which is of the order of a few hundred kelvin for the isothermal sintering but only a few tens of Kelvin for the second case. As the process of surface diffusion is known to be thermally activated, the temperature insensitivity at the stage of rapid necking implies that instead of surface diffusion, the elasto-plastic deformation induced by the large interatomic interactions is more likely to play the predominant role as observed in the previous studies as well [7,10]. Thereafter, we find a temperature dependent stage of neck-growth, where the distance between the AuNPs fluctuates, thereby causing fluctuations in the radius of gyration of the two-particle system. Interestingly, this “breathing” phenomenon also manifests in the profiles of principal coordinates (Fig. 1) in the form of oscillations. During the isothermal sintering (Fig. 1a), these oscillations are comparatively more prominent at 550K

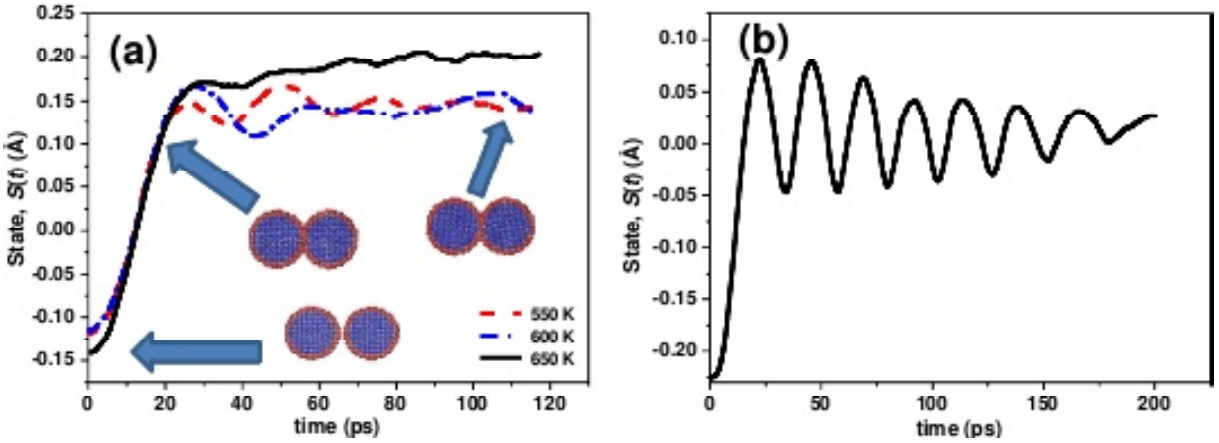

Fig. 1. Principal projection versus time for sintering under (a) isothermal conditions and (b) linear rise in temperature. Typical snapshots of the AuNP systems are also shown with the plots.

and 600K. On the other hand, at the larger temperature of 650K, such oscillations are hardly noticeable and indicate that temperature has a damping effect on breathing. This general trend helps us to understand the behavior in the second case of linear heating (Fig. 1b), where we find that significantly large oscillations are obtained, which gradually decrease with time. This is attributable to the linearly rising temperature because of which, the temperature remains below 350K for the first 100 ps and the damping is not strong enough to sufficiently reduce the amplitudes of the oscillations. The observation of oscillations and subsequent damping can be accounted for by taking into consideration the interplay of two different modes of necking during the process of nanosintering. At one hand, the deformation of the nanoparticles due to direct inter-particle interaction during the first few picoseconds has a significant elastic component, which induces elastic strain in the system [10]. As soon as the elimination of surfaces take place due to contact between the AuNPs, this elastic strain tends to get released and sets oscillations due to the intrinsic inertia of the particles. At the other hand, curvature-driven diffusion causes the atoms on the surfaces to migrate towards the neck, which enhances the adhesion between the AuNPs. As the process of diffusion is an irreversible one, it possesses an inherent tendency of damping the oscillations. Moreover, the increase in surface diffusivity with temperature explains why the oscillations of the principal component $S(t)$ are largely damped at higher temperature.

Evaluating the rate of a process is a key component of the study of its kinetics. In the present scenario, compression of the multivariate state, $\mathbf{s}(t)$, to a single variable, $S(t)$, greatly facilitates the calculation of the rate of nanosintering. Here we define the rate of the process simply as, $R(t) = \mathrm{d}S(t)/\mathrm{d}t$. It must be pointed out that due to the discrete nature of the simulation data, even a minute roughness in the profile of $S(t)$ can lead to very large values of the time-derivative. This inherent artefact of numerical differentiation, if arises, can be bypassed by smoothening the $S(t)$ profile by means of cubic-spline interpolation to fill the gap between the discrete points, followed by the FFT based smoothening. The rates for both the modalities of sintering simulated in this study have been calculated and plotted in Fig. 2. The first stages of rapid neck initiation are identified as peaked profiles with their maxima lying in the range of about 10 – 12 ps for all the simulations. Subsequently, the rates oscillate in a manner similar to the state $S(t)$ in Fig. 1, and can become negative on account of the breathing phenomenon. In contrast to the isothermal sintering (Fig. 2a), linear heating (Fig. 2b) causes $R(t)$ to swing over a much larger range during the second stage.

In order to perceive the process of necking from a thermodynamic standpoint, the energetics associated with the process must be taken into consideration. Fig. 3a shows the typical variation of the structural energy, $U(t)$, of the AuNP systems as the functions of time for isothermal sintering. We can find that here again, the first stage of necking is recognized as the initial rapid decline in the structural energy of the system. This drop continues for ~10 – 12 ps, *i.e.*, till the rate becomes maximum as displayed in Fig. 2a. For the next 10 ps, a plateau-like region is obtained which extends to the onset of the second stage and afterwards, reduction in $U(t)$ takes place at a decreasing rate due to the slower process of surface elimination. At this point, it is of interest to note that these two stages

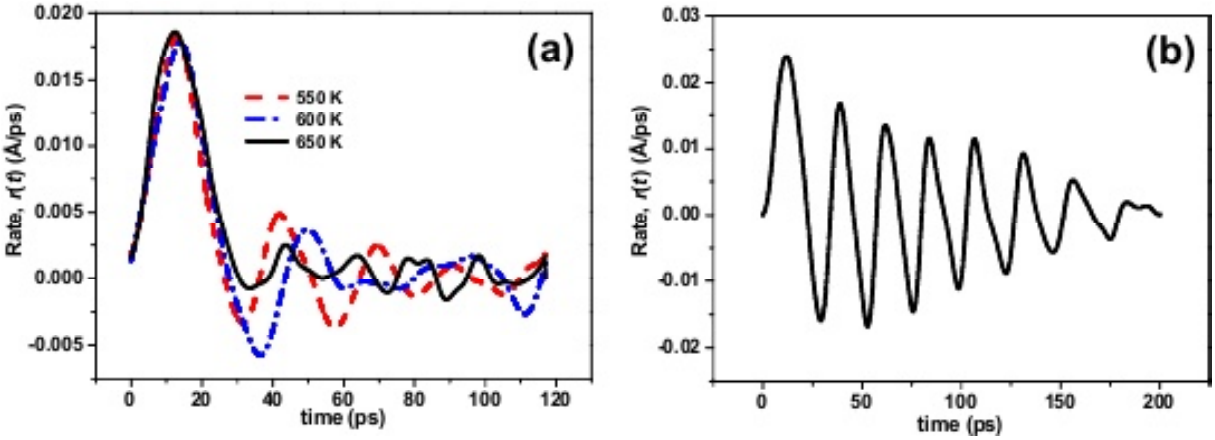

Fig. 2. Instantaneous rates of the nanosintering processes for (a) isothermal sintering and (b) linear heating. Negative rates indicate increasing separation between the nanoparticles during the breathing phenomenon.

characterized by different rates and temperature-sensitivities (Figs. 1 and 2) can also be identified in the evolution of parameters like neck-size and densification during the sintering of copper nanofibres [26]. In particular, the general trend of $U(t)$ as shown in Fig. 3a shows an excellent resemblance with the qualitative behaviour of densification as given in Fig. 5b of Ref. [26]. Energetics of the isothermal nanosintering can further be understood by considering the structure and dynamics of the process at different instants of time. The initial fast drop of the structural energy is caused by the effect of surface elimination, but at the same time, the two-particle system gets squeezed in the process. As mentioned earlier, the temperature is sufficient to activate the surface-diffusion and the extra adhesion between the particles resists the release of the trapped strain energy. This nullifies the rapid decline of $U(t)$ in the initial stage and yields the plateau-like region (Fig. 3a). As the trapped stress in the system becomes too large, it nucleates partial dislocations which rapidly slide across the interface and release the stress, leaving behind their trails in the form of stacking faults. Once the stored energy is removed through plastic deformation of both the nanoparticles, the potential energy starts decreasing in the usual manner. This modality of sintering is illustrated in Fig. 3b, where the elasto-plastic mechanism is clearly revealed.

In stark contrast to isothermal sintering, linear heating exhibits a qualitatively different variation of the structural energy. In this case, the rising temperature of the system imparts a gradually increasing thermal energy, which is partitioned equally between the potential and kinetic modes. This thermal component is superposed on the usual reduction in structural energy due to sintering, and results in the net potential energy of the system. As the thermostat causes the thermal energy to increases linearly with time irrespective of the state of the AuNP system, we must filter out this thermal

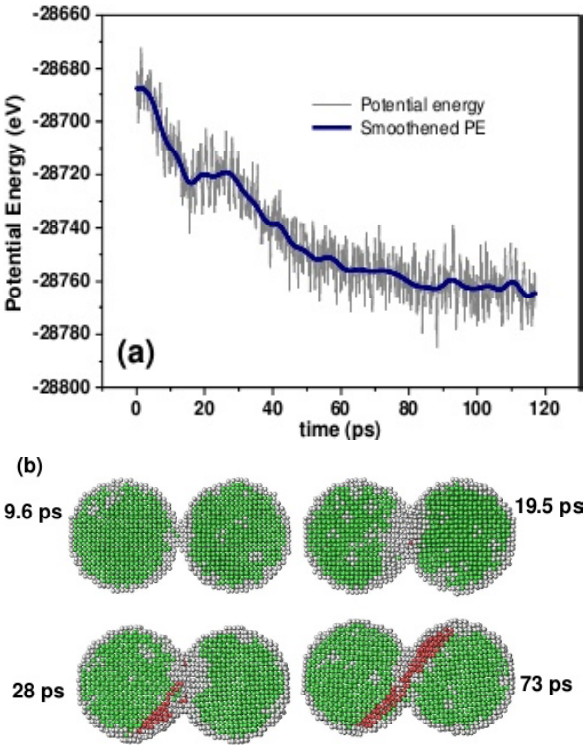

Fig. 3. (a) Typical variation of the potential energy of the AuNP system at 650K isothermal sintering along with a smoothened profile obtained by removing the high frequency thermal fluctuations and (b) the cross-sectional view of the nanoparticles at different instants of time. The red atoms belong to the stacking faults created as the outcome of plastic slips.

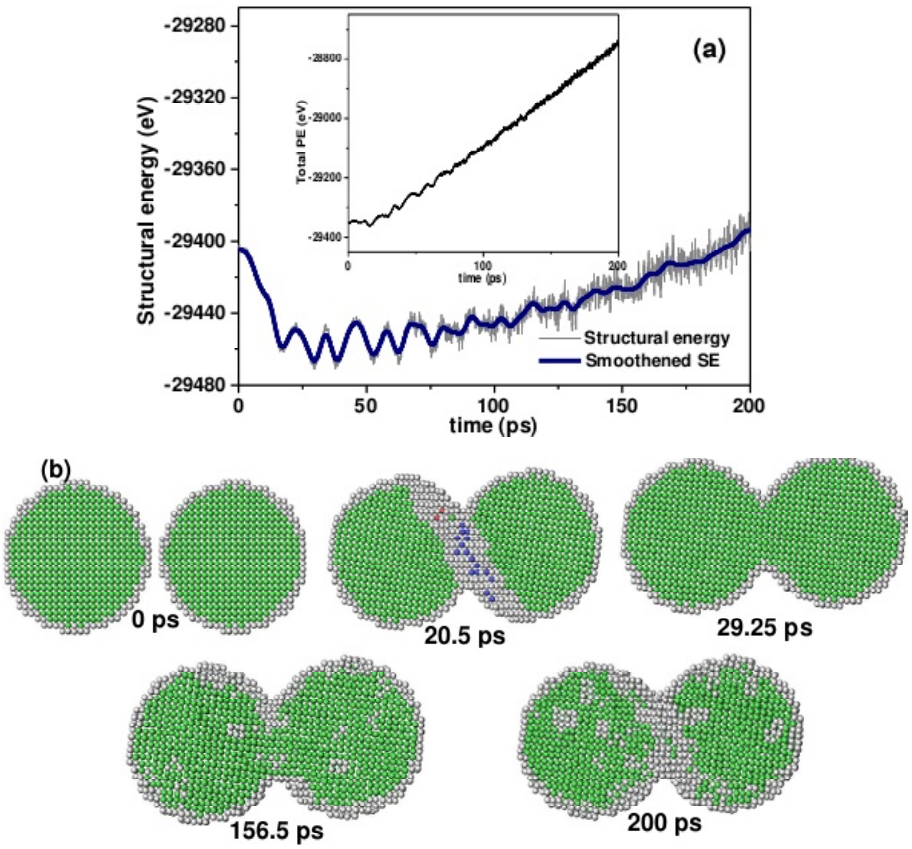

Fig. 4. Structural energy of the nanoparticles during linear rise in temperature, plotted against the sintering time. This is obtained by removing the thermal energy from the net potential energy, which is shown in the inset.

component (3/2 k*T*/atom) and consider only the structural energies of the particles. Fig. 4a shows the structural energy of the nanoparticles after deducting the thermal part from the total potential energy (inset). We observe an initial sharp fall in the structural energy followed by wavy variation for about 75-ps. Later on, instead of showing the regular reduction, the structural energy starts increasing. Akin to that in Fig. 3b, the mechanism of sintering for the present case is displayed in Fig. 4b. We can see that when the particles get squeezed during the breathing process, the atoms at the interface between the AuNPs get distorted, causing a rise in the structural energy. Nevertheless, in absence of sufficient surface-diffusion and interparticle adhesion, the system tends to revert back to release the trapped stress and distortions of the interfacial structure. This causes the energy oscillations observed in Fig. 4a. At a later stage, the rising temperature becomes large enough to start disturbing the crystalline structure at the neck (Fig. 4b), causing futher rise in the structural energy. Here it can be appropriate to point out that the principal projections shown in Fig. 1 show much cleaner profiles than those of $U(t)$ in Figs. 3a and 4a, where the high frequency thermal noises are evident. Such an effect is attributable to the fact that in contrast to $U(t)$, $S(t)$ is obtained after removing the contributions corresponding to the non-principal eigenvalues obtained from the original dataset $\mathbf{s}(t)$. Absence of fluctuations in the profiles of $S(t)$ is an excellent demonstration of the noise filtering capability of PCA as mentioned in Sec. 3.

As we have been able to evaluate not only the single variable state representing the multivariate data but the evolution of the potential energy as well, it is now possible to make sense of an effective "thermodynamic force". We can define this quantity in terms of the state derivative of the potential energy as, $F = -\mathrm{d}U/\mathrm{d}S$. For the purpose of calculating the derivatives, smoothened profiles of $U(t)$ have been used in order to avoid the spurious effects created by the thermal noise. In case of the linear rise in temperature, $U(t)$ must be the structural energy obtained after removing the thermal part from the net potential energy as explained above. However, this filtering is not essential for the isothermal sintering, for the thermal energy remains invariant with respect to change in state throughout the simulation. The thermodynamic forces computed by this

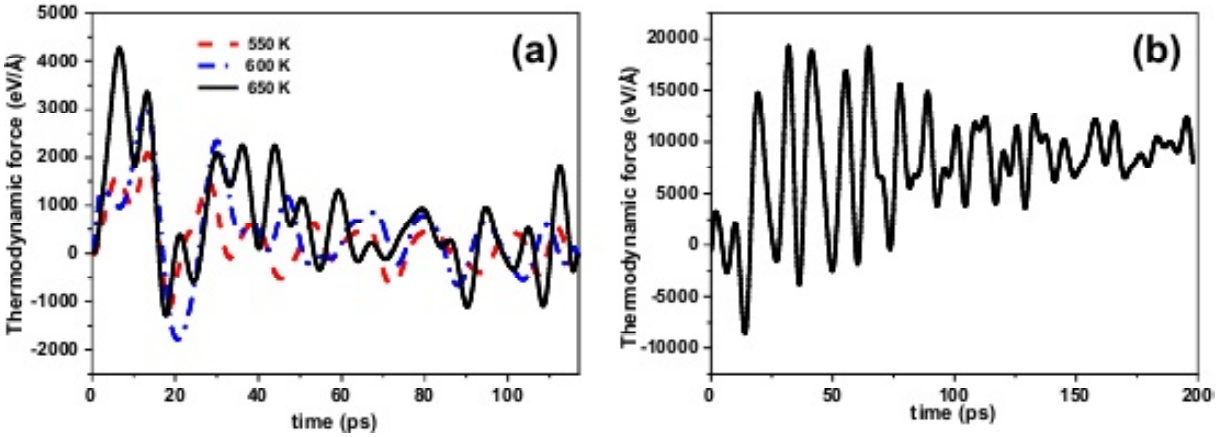

Fig. 5. One-dimensional effective thermodynamic force on the system of two nanoparticles undergoing the process of sintering at (a) constant and (b) linearly rising temperature.

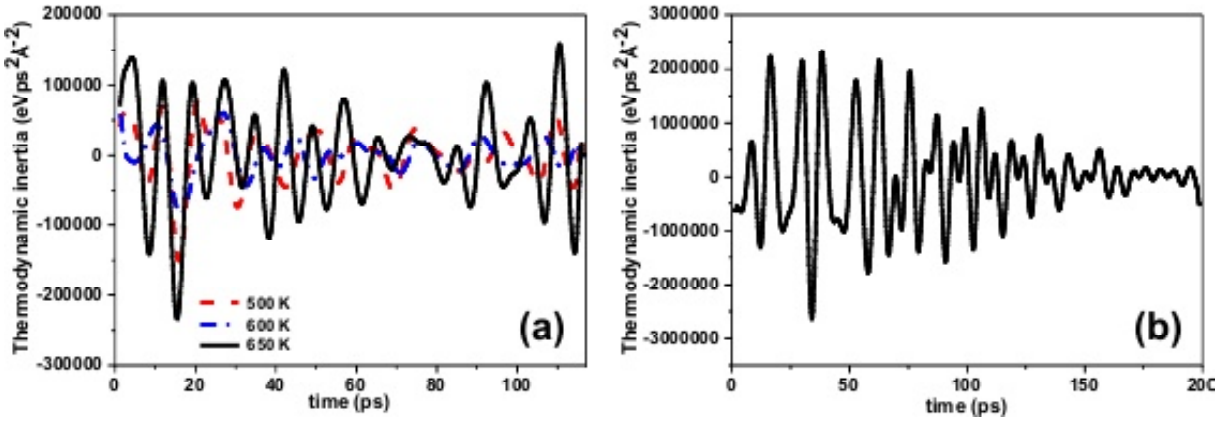

Fig. 6. Evolution of the effective thermodynamic inertia with time for the cases of (a) isothermal sintering and (b) ramp heating of the pair of AuNPs.

method are oscillating throughout the process. During the first stage of isothermal sintering (Fig. 5a), the forces vary over a large range and even become negative on account of the breathing phenomenon. During the initial stage, the forces rise rapidly in the positive direction, attain their maxima and then suddenly drop to large negative minima at ~ 20 ps near the end of the first stage. In the second stage, the effective thermodynamic forces correspond to the mechanism of curvature driven surface diffusion, and are smaller than the forces due to direct inter-particle interactions causing elasto-plastic deformation of the AuNPs. This modality of the kinetics is responsible for a different trend of thermodynamic forces in the case of linear heating as displayed in Fig. 5b. Here we find that the oscillations are much more prominent for the first 100 ps, *i.e.*, the duration during which the temperature is not large enough to excite the surface diffusion to a significant extent. Later on, the surface diffusion increases and the damping of $S(t)$ oscillations (Fig. 1b) entails the oscillations of $F(t)$ to subside.

As the approach of employing the tool of dimensionality reduction provides one-dimensional (or scalar) equivalents of the otherwise vector quantities, it also enables us to define the effective thermodynamic inertia of the AuNP system simply as,

$$m(t) = \frac{\mathrm{d}F(t)}{\mathrm{d}\left\{\mathrm{d}^2 S(t)/\mathrm{d}t^2\right\}}.$$

Interestingly, this effective inertia or mass of the system does not remain static, but vary vigorously over very large ranges as evident from their plots displayed in Fig. 6. As a matter of fact, this behaviour is not unexpected because in contrast to the conventional notion of mass, the thermodynamic inertia actually represents the collective response of a many-body system to the thermodynamic forces. Thus, the overall value of $m(t)$ consists of the actual masses of the AuNPs, in addition to the effect of instantaneous structure of the system. Although the masses of the particles remain fixed, the instantaneous structure gradually evolves in time through the mechanisms of surface diffusion and elasto-plas-

tic deformation, thereby making the effective inertia a time-variant parameter. As the thermodynamic force, $F(t)$, and the structural state, $S(t)$, represent the compressed behaviour of a multi-dimensional system, various mechanisms involved in the dynamics simultaneously affect their values and can make $F(t)$ and $S(t)$ vary out of phase in time. When it happens, the thermodynamic inertia shows negative values at several instances as illustrated in Fig. 6.

Hence, by obtaining the principal component of the multivariate trajectory, $S(t)$, and the evolution of the structural energy, $U(t)$, it becomes possible to compute the effective thermodynamic inertia, which reflects not only the mechanical masses of the individual components, but the structural configuration of the system as well.

5. CONCLUSIONS

By the way of summary, this paper proposes the use of dimensionality reduction as a means for better comprehension of the thermodynamics and kinetics of a complex process. A linear process of dimensionality reduction, namely, the principal component analysis has been employed to demonstrate the feasibility of this concept. As the case study, sintering of two gold nanoparticles have been simulated by molecular dynamics methods under the conditions of isothermal and ramp heating. These simulations have uncovered the fundamental differences in the energetics and kinetics of the sintering process for both types of heating and furnished valuable insight of the breathing phenomenon. Calculations reveal that the principal components of multivariate atomic trajectories in these simulations correspond to large eigenvalues, thereby underscoring the efficacy of PCA in such studies. It is shown that when the energetics of a process is obtained in conjunction with the principal projection of the original dataset of atomic coordinates, it is possible to define and compute meaningful quantities like effective thermodynamic force and inertia, which being single variable quantities, can be simple and subject to intuitive interpretations. The fact that the method of PCA can even act as an absolute blind analyzer not requiring any *a priori* detail of the system setup, makes the principal component of the atomic trajectories a more preferable logical choice over any other parameter directly measurable from the simulations. Even though the exact details of the technique of dimensionality reduction can be customised according to the specifications of the system and process under investigation, the underlying principle is more fundamental and therefore applicable to a wide range of studies.

ACKNOWLEDGEMENTS

The author thanks the DST (Govt. of India) for providing financial support for this work under the DST-INSPIRE faculty scheme.

REFERENCES

[1] S. Jang, Y. Seo, J. Choi, T. Kim, J. Cho, S. Kim and D. Kim // *Scr. mater*. **62** (2010) 258.
[2] A. Hu, J.Y. Guo, H. Alarifi, G. Patane, Y. Zhou, G. Compagnini and C.X. Xu // *Appl. Phys. Lett*. **97** (2010) 153117.
[3] D. Tobjörk, H. Aarnio, P. Pulkkinen, R. Bollström, A. Määttänen, P. Ihalainen, T. Mäkelä, J. Peltonen, M. Toivakka and H. Tenhu // *Thin Solid Films* **520** (2012) 2949.
[4] S.C. Parker and C.T. Campbell // *Phys. Rev. B* **75** (2007) 035430.
[5] F. Behafarid and B.R. Cuenya // *Surf. Sci.* **606** (2012) 908.
[6] V.N. Koparde and P.T. Cummings // *J. Phys. Chem. B* **109** (2005) 24280.
[7] H. Pan, S.H. Ko and C.P. Grigoropoulos // *J. Heat Transf.* **130** (2008) 092404.
[8] P. Song and D. Wen // *J. Nanopart. Res*. **12** (2010) 823.
[9] V. Mukundan, B.N. Wanjala, R. Loukrakpam, J. Luo, J. Yin, C.J. Zhong and O. Malis // *Nanotechnology* **23** (2012) 335705.
[10] H. Zhu // *Phil. Mag. Lett.* **73** (1996) 27.
[11] A. Moitra, S. Kim, S.-G. Kim, S.J. Park, R.M. German and M.F. Horstemeyer // *Acta Mater*. **58** (2010) 3939.
[12] L. Ding and R.L. Davidchack and J. Pan // *Comp. Mater. Sc*i. **45** (2009) 247.
[13] T. Hawa and M.R. Zachariah // *Phys. Rev. B* **76** (2007) 054109.
[14] J. Li, S. Sarkar, W.T. Cox, T.J. Lenosky, E. Bitzek and Y. Wang // *Phys. Rev. B* **84** (2011) 054103.
[15] S. Arcidiacono, N.R. Bieri, D. Poulikakos and C.P. Grigoropoulos // *Int. J. Multiphas. Flow* **30** (2004) 979.
[16] J.B. Adams, S.M. Foiles and W.G. Wolfer // *J. Mater. Res.* **4** (1989) 102.
[17] S. Nosé // *J. Chem. Phys*. **81** (1984) 511.
[18] W.G. Hoover // *Phys. Rev. A* **31** (1985) 1695.
[19] S.J. Plimpton // *J. Comp. Phys.* **117** (1995) 1.
[20] I.T. Jolliffe, *Principle Component Analysis* (Springer-Verlag, New York, 2002).
[21] J. Hasbrouck and D.J. Seppi // *J. Financial Econ*. **59** (2001) 383.

[22] Y. Okamoto, T. Kajimura, T.M. Ikeda and S. Takumi // *Genes Genet. Syst.* **87** (2012) 299.
[23] K.I. Kim, M.O. Franz and B. Schölkopf // *IEEE Trans. Pattern Analysis and Machine Intell.* **27** (2005) 1351.
[24] S.V. Kalinin, B.J. Rodriguez, J.D. Budai, S.Jesse, A.N. Morozovska, A.A. Bokov and Z.G. Ye // *Phys. Rev. B* **81** (2010) 064107.
[25] M. Bhattacharya, A. Dutta and P. Barat // *Phys. Rev. B* **87** (2013) 214107.
[26] P. Zeng, S. Zajac, P.C. Clapp and J.A. Rifkin // *Mater. Sci. Engg. A* **252** (1998) 301.